Supporting Information

Eco-Friendly Photochemical Production of H_2O_2 through O_2 Reduction over Carbon Nitride Frameworks Incorporated with Multiple Heteroelements

Gun-hee Moon,[†] Mamoru Fujitsuka,[‡] Sooyeon Kim,[‡] Tetsuro Majima,[‡] Xinchen Wang,[§] and Wonyong Choi[*,†]

[†]*Department of Chemical Engineering & Division of Environmental Science and Engineering, Pohang University of Science and Technology (POSTECH), Pohang, 37673 Korea*

[‡]*The Institute of Scientific and Industrial Research (SANKEN), Osaka University, Osaka 567-0047, Japan*

[§]*College of Chemistry, Fuzhou University, Fuzhou 350002, P. R. China*

* To whom correspondence should be addressed (W. Choi)

E-mail: wchoi@postech.edu Fax: +82-54-279-8299

Experimental Details

Materials Characterizations

Powder X-ray diffraction (XRD) patterns were measured by a PANalytical X'Pert diffractometer with an X'Celerator detector using Cu K_a line (1253.6 eV). The morphology was measured by field emission scanning electron microscopy (FE-SEM, JEOL, JSM). Transmission electron microscopy and EDX mapping/spectra were taken by JOEL JEM-2200FS (with Image Cs-corrector). The functional groups of all samples were recorded by Attenuated total reflectance Fourier transform infrared spectroscopy (ATR-FTIR, Thermo Scientific iS50) using ZeSe crystal. The number of scan was 100 and the resolution was 4 cm^{-1}. Diffuse reflectance UV/visible absorption spectra (DRUVS) were obtained by Shimadzu UV-2401PC with an integrating sphere attachment. Before measurement, $BaSO_4$ (Junsei) was used as a reference. The UV/Visible absorbance of H_2O_2 solution was obtained by a UV/Visible spectrophotometer (Agilent 8453).

Zeta potential of the aqueous suspension was measured using an electrophoretic light scattering spectrophotometer (ELS 8000, Otsuka). Before the measurement, all samples were sonicated in ultrasonic bath to disperse in water, and then the pH of the aqueous suspension was adjusted by $HClO_4$ and KOH. All points were measured three time and the values were averaged. Thermogravimetric analysis (TGA) was performed on an SII EXSTAR 6000 thermal analyzer. The samples were heated under air atmosphere from room temperature to 930 ^oC with a heating rate of 2 ^oC/min. The BET surface areas of all samples were measured from the nitrogen adsorption/desorption isotherms (Tristar II 3020, Micromeritics Instrument Corporation) after pre-treatment at 50 ^oC in vacuum for 12 h.

X-ray photoelectron spectroscopy (XPS) analysis were performed by ESCALAB 250 XPS System (Thermo Fisher Scientific, UK) with an X-ray source using monochromatic Al Kα (1486.6 eV). The XPS elemental analysis was corrected based on the C1s peak at 284.6 eV. The deconvolution and curve fitting were done using eXPFit software (version 1.5). Elemental analysis of the samples was performed with an Elementar Vario MICRO Cube (Elementar Analysensysteme GmbH, Germany). The solid-state ^{31}P MAS NMR spectra were collected at 600 MHz (14.1 T) using ^{unity}INOVA, (Agilent Technologies, U.S.A) with a 2.5mm HX-MAS probe. The spinning rate was 25 kHZ and the pulse width was 1.7 µs (45^{o} pulse). The chemical shift of P was expressed in ppm relative to 85% H_3PO_4 solution. The solid-state ^{13}C CPMAS NMR spectra were collected at 600 MHz (14.1 T) using ^{unity}INOVA, (Agilent Technologies, U.S.A) with a HX-CPMAS probe. The spinning rate was 10 kHZ and the Larmor frequency was 105.883 MHz. The proton π/2 pulse was 5 µs the contact time for CP was 3 ms.

Photoluminescence (PL) emission and excitation spectra were collected at room temperature with a fluorescence spectroscopy (Shimadzu RF-5301). The experimental set-up for time-resolved diffuse reflectance spectra was same as described in our previous paper.[1] In this study, the sample coated on glass substrate was excited with a 400 nm femtosecond laser pulse (~ 3µJ per pulse).[2]

For Mott-Schottky measurement, the samples were coated on a fluoride tin oxide (FTO) glass by a Doctor blade method. The electrochemical performance was measured by a three electrode system under Ar-purged system. Pt wire, graphite rod, and Ag/AgCl were utilized as a working electrode, a counter electrode, and a reference electrode, respectively, which were connected to a potentiostat (Gamry, Reference 600). The pH was adjusted to 7.0 and 0.1 M of Na_2SO_4 was added. The slurry-type photocurrent was measured with a three-electrode system consisting of Pt, counter,

and Ag/AgCl electrode. The phosphotungstate redox couple acting as an electron shuttle transfers the electrons generated on the photocatalyst to a Pt electrode under continuous Ar-purged condition. Photocatalyst suspension (0.5 g/L) with 2.0 mM of sodium phosphotungstate (an electron shuttle) and 0.1 M of $NaClO_4$ (electrolyte) at pH 3 was irradiated by a 300-W Xe arc lamp with a UV cutoff filter ($\lambda \geq 420$ nm). Photocurrent was collected with a Pt electrode held at +0.7 V (vs Ag/AgCl).

H_2O_2 measurement

Specific amount of sample aliquots was collected by a syringe and filtered by 0.45 μm PTFE filter (Millipore). To make N,N-diethyl-1,4-phenylene-diamine sulfate (DPD, 97%, Aldrich) and peroxidase (POD, horseradish, Aldrich) stock solution, 0.1 g of DPD was dissolved in 10 mL of 0.1 N H2SO4 solution and 3 mg of POD was dissolved in 3 mL of purified water, respectively. Phosphate buffer solution was prepared by mixing of monobasic sodium phosphate (Aldrich) solution (87.7 mL of 1 M), dibasic sodium phosphate heptahydrate (Aldrich) solution (12.6 mL of 1 M), and 99.7 mL of purified water. Specific amount of sample aliquots and purified water was mixed with 0.4 mL of phosphate buffer, 0.05 mL of DPD, and 0.05 mL of POD, which was kept under vigorous stirring for 90 s (2.67 mL of total volume). The absorbance was measured at 551 nm by UV/visible spectrophotometer. The calibration for each H_2O_2 concentration was performed by dilution of 30 wt.% H_2O_2 solution (Junsei).

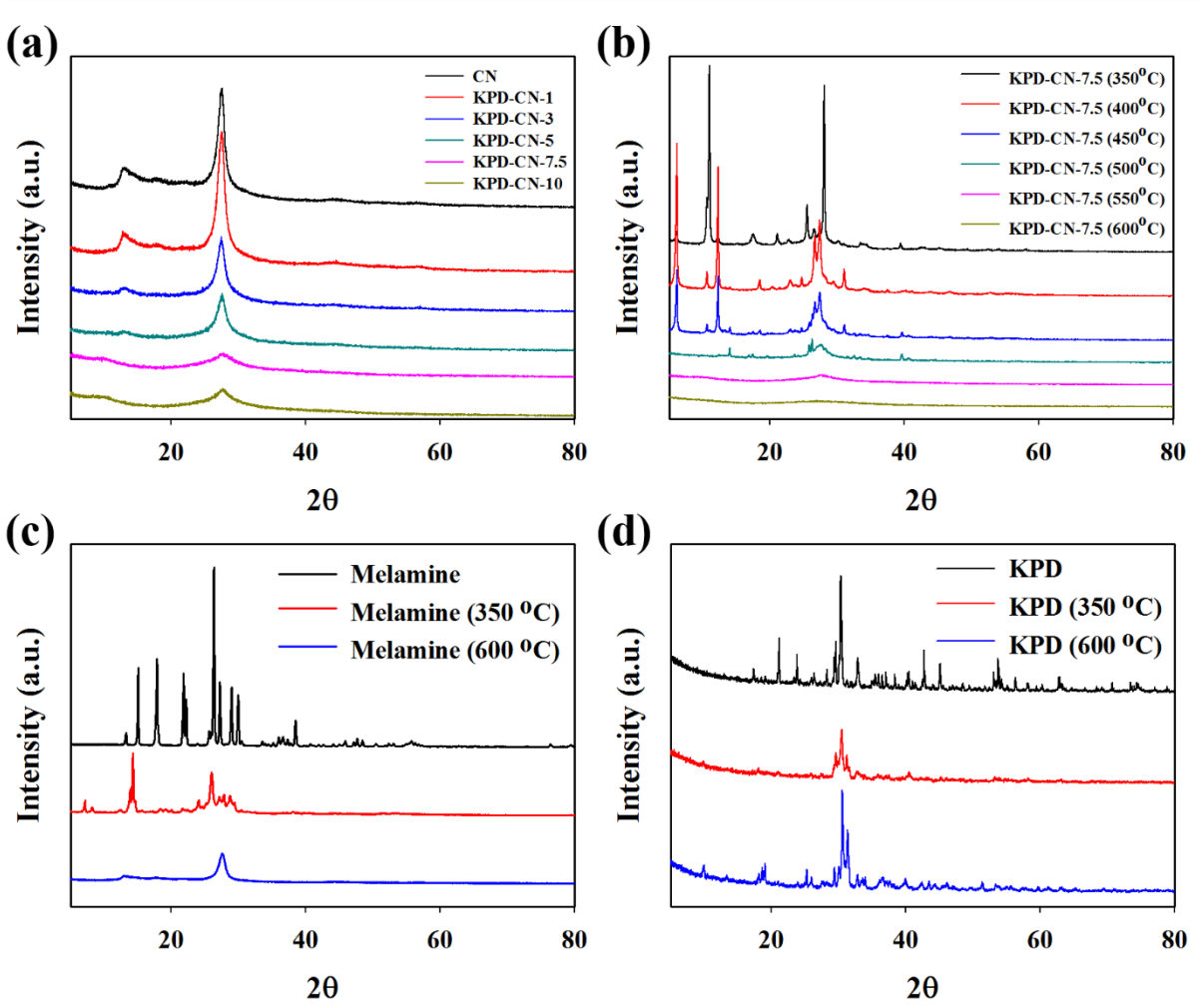

Figure S1. (a) XRD patterns of bare CN with varying KPD content, (b) XRD patterns of KPD-CN-7.5 depending on the calcination temperature, (c) XRD patterns of melamine after calcination at 350 and 600 °C, (d) XRD patterns of KPD after calcination at 350 and 600 °C.

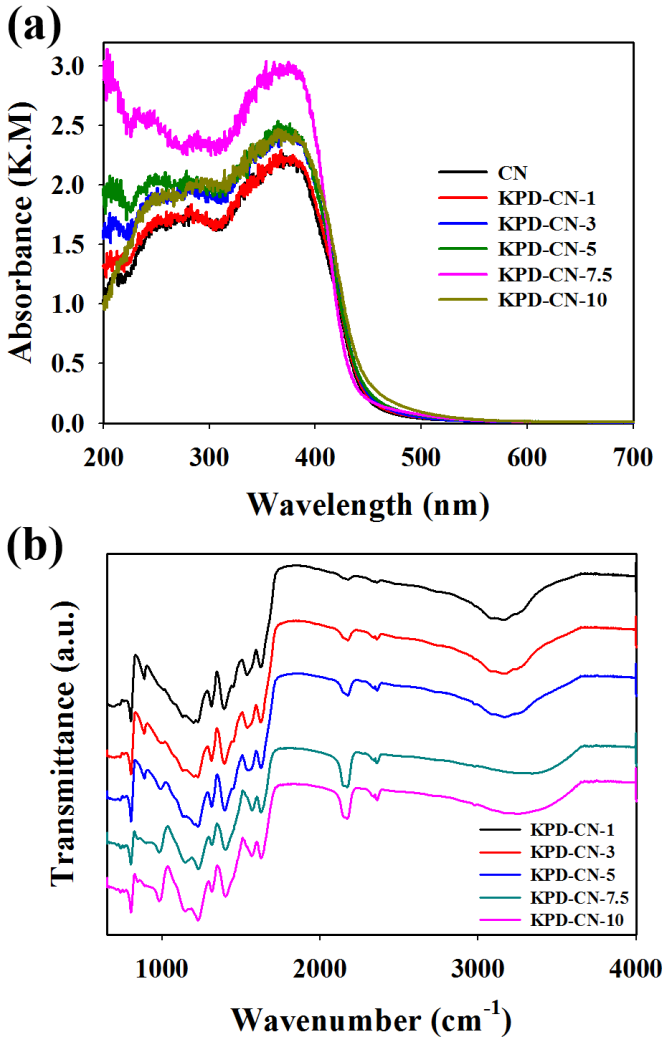

Figure S2. (a) DRUVS spectra of KPD-CN-x (x=0, 1, 3, 5, 7.5, and 10) and (b) ATR-FT-IR transmittance spectra of KPD-CN-x (x=1, 3, 5, 7.5, and 10).

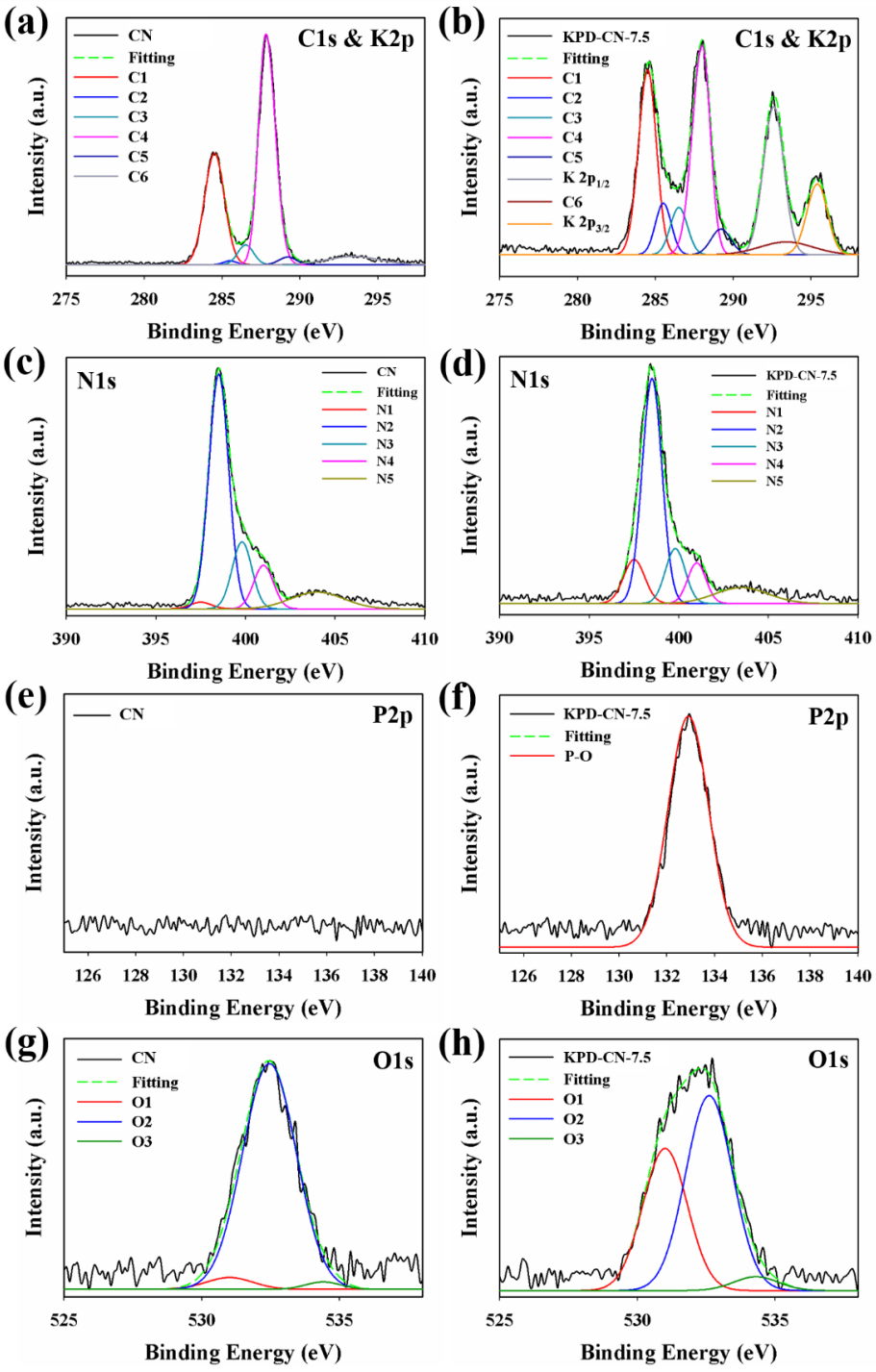

Figure S3. Deconvoluted XPS core-level spectra of (a & b) C1s and K2p, (c & d) N1s, (e & f) P2p, (g & f) O1s for bare CN (a, c, e, and g) and KPD-CN-7.5 (b, d, f, and h). Black line is an original data and the green line is a curve fitting result.

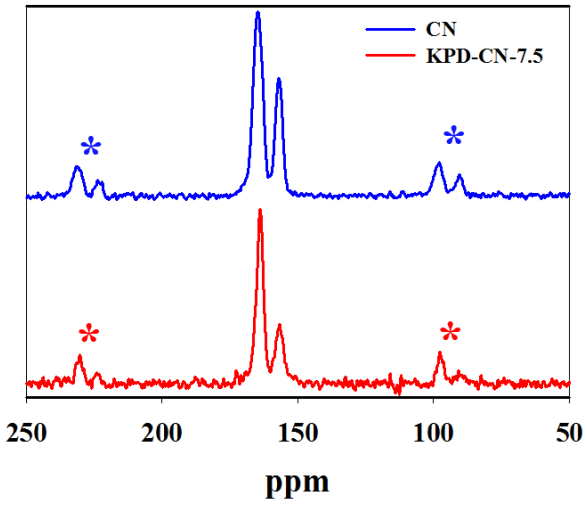

Figure S4. Proton-decoupled ^{13}C CP-MAS NMR spectra of bare CN and KPD-CN-7.5.

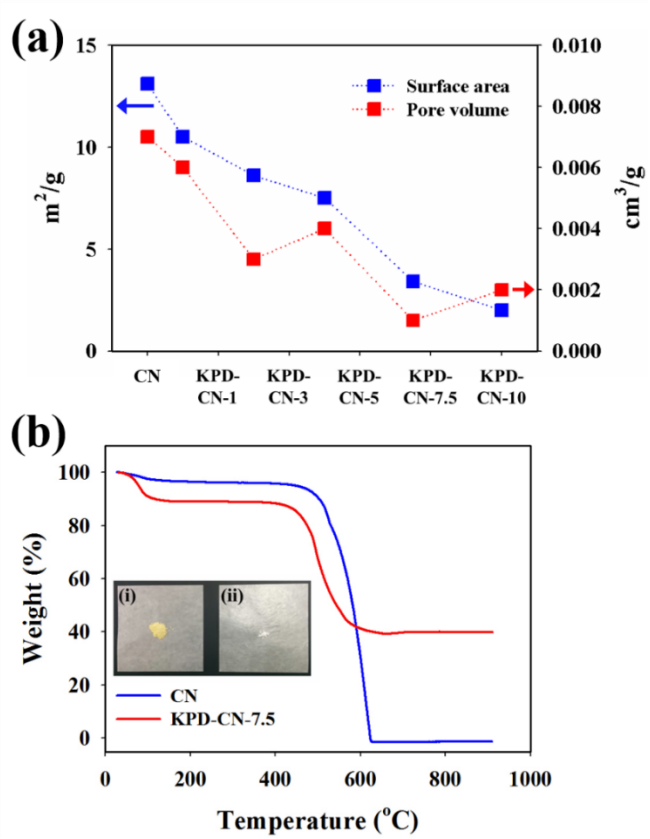

Figure S5. (a) The BET surface area (Left axis) and pore volume (Right axis), (b) TGA curves of bare CN and KPD-CN-7.5. Inset in (b): The photograph of KPD-CN-7.5 before (i) and after heat treatment at 900 °C in air (ii).

The BET surface area and pore volume steadily decreased with increasing the KPD content (Figure S5a). Even though many studies have reported that the chemical treatment of the precursor of bare CN using sulfuric acid, barbituric acid as an organic monomer, and alkali metal ions brings about the increase of the surface area accompanying the change of morphology,[3-5] the utilization of KPD results in the decrease of the surface area. The TGA plots demonstrate that the KPD-CN-7.5 was less thermally stable than the bare CN in air (a platinum crucible without a cap), and more water molecules adsorbed on the surface of KPD-CN-7.5 were detected (Figure S5b). Above 600 °C, all CN were decomposed to CO_2 and NH_3 but about 40 % of KPD-CN-7.5 still remained even at 900 °C, which indicates that 40 % of KPD-CN-7.5 is ascribed to potassium phosphate complexes.

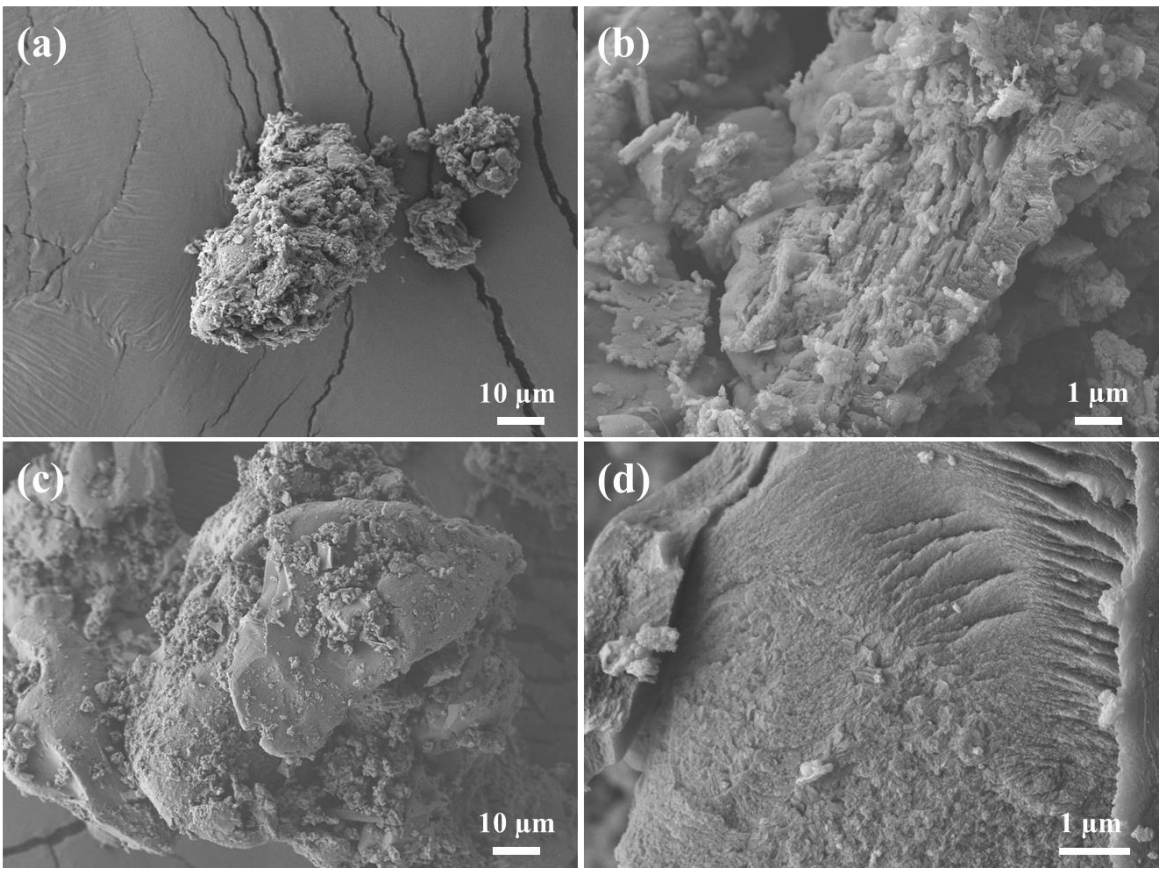

Figure S6. FE-SEM images of (a, b) bare CN and (c, d) KPD-CN-7.5 with different magnification.

The phosphate moieties on the CN matrix can play a role as not only a binder among other tris-s-triazine moieties through hydrogen bonding of $–NH_2$ groups[6-8] but also a chelating agent for the strong coordination with potassium ions together with non-pair electrons of nitrogen atoms. Therefore, the graphitic structure of CN is broken through angular distortion by phosphate species and then by random stacking of polymeric tris-s-triazine layers as already shown in XRD analysis. Field-emission scanning electron microscopy (FE-SEM) image shows that the particle size of KPD-CN-7.5 was visibly larger than that of bare CN, and the pores present in CN were densely packed and vanished in KPD-CN-7.5 (see Figure S5a).

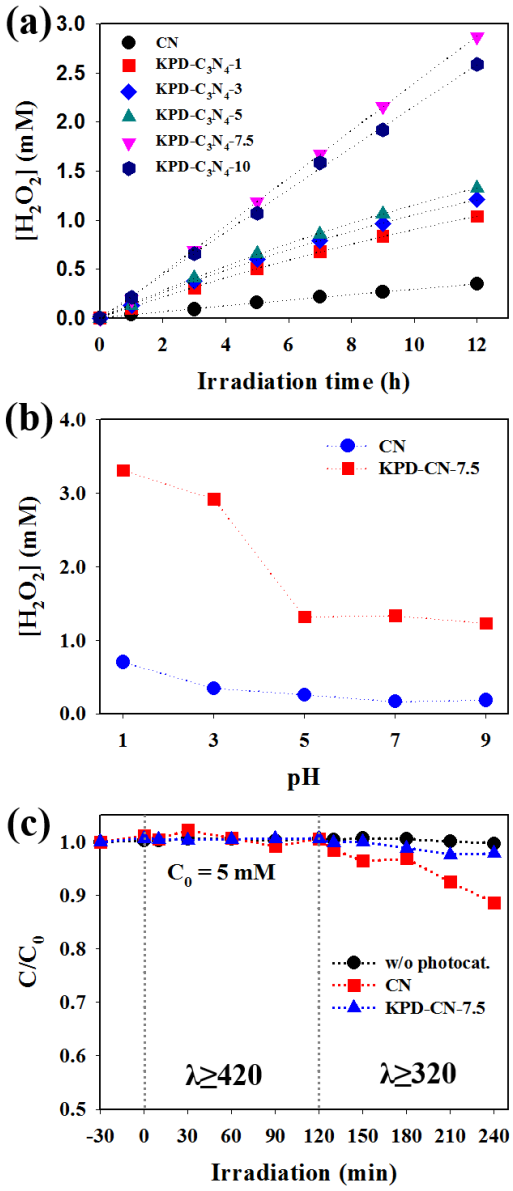

Figure S7. (a) Comparison of the photocatalytic formation of H_2O_2 under O_2-equilibrated conditions with increasing KPD content. The experimental conditions were as follows: 0.5 g/L of photocatalyst, 10 vol.% of ethanol, pH_i = 3.0, and $\lambda \geq 420$ nm. (b) The effect of pH on the production of H_2O_2 for bare CN and KPD-CN-7.5. (c) The photocatalytic decomposition of H_2O_2 for bare CN and KPD-CN-7.5. The experimental conditions were as follows: 0.5 g/L catalyst, $[H_2O_2]_i$ = 5 mM, pH_i = 3, $\lambda \geq 420$ nm, and $\lambda \geq 320$ nm.

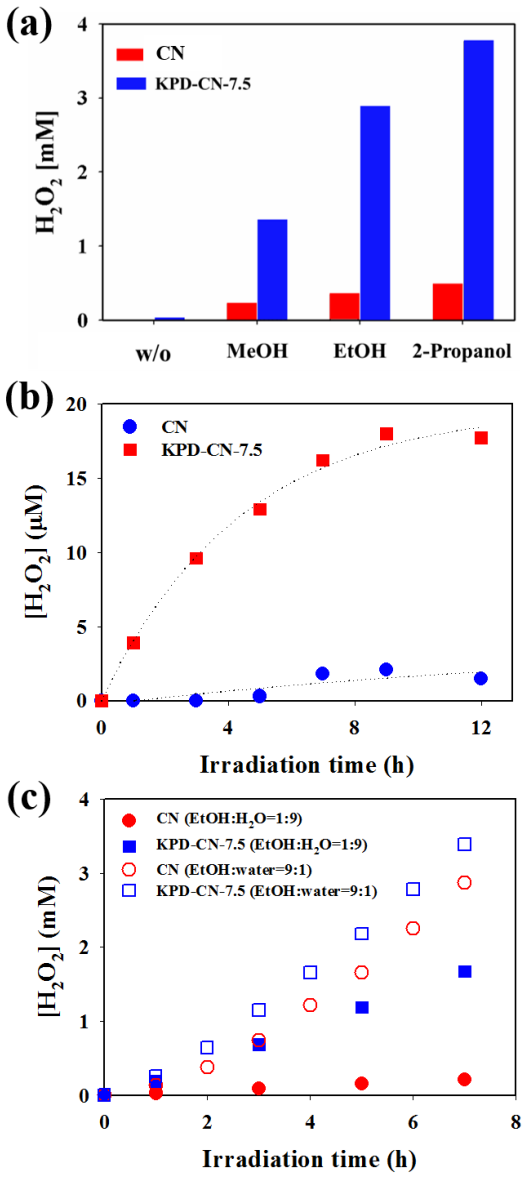

Figure S8. (a) The effect of electron donor on the photocatalytic production of H_2O_2 (at 12 h) under O_2-equilibrated condition for bare CN and KPD-CN-7.5. The experimental conditions were: 0.5 g/L of photocatalyst, 10 vol.% of alcohol, pH_i = 3.0, and $\lambda \geq 420$ nm. (b) The formation of H_2O_2 in the absence of electron donor for bare CN and KPD-CN-7.5. (c) The production of H_2O_2 in different mixtures of water and ethanol (10% *vs.* 90% EtOH) for CN and KPD-CN-7.5. The experimental conditions were: 0.5 g/L of photocatalyst, pH_i = 3.0, and $\lambda \geq 420$ nm.

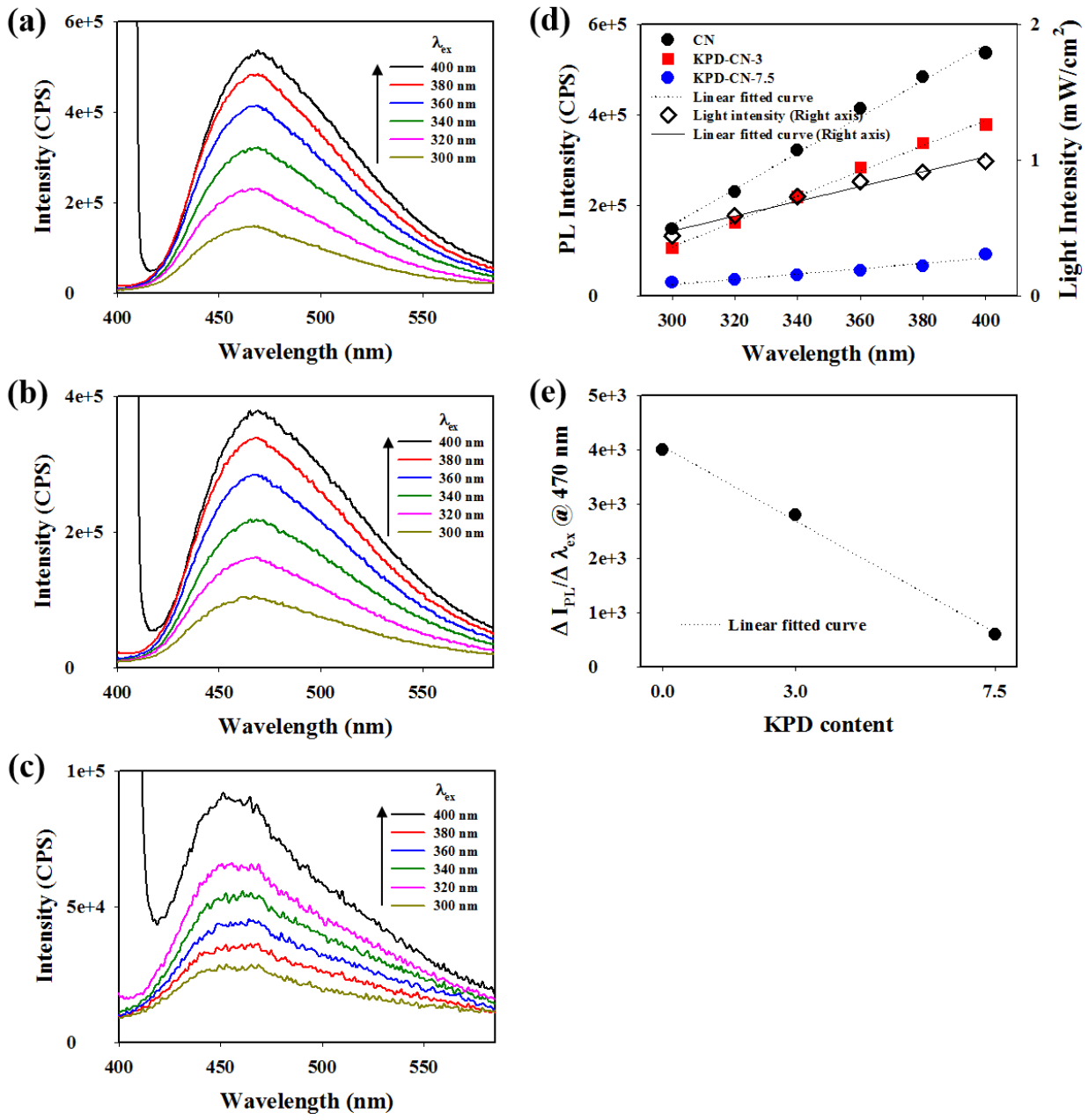

Figure S9. PL emission spectra depending on the excitation wavelength for (a) bare CN, (b) KPD-CN-3, and (c) KPD-CN-7.5. (d) Excitation wavelength-dependent PL emission intensity at 470 nm (left) and excitation light intensity (right). (e) Slope change with increasing KPD content.

Table S1. FT-IR spectra of bare CN and KPD-CN-7.5.[3, 9-15]

Sample	No.	Frequency	Type of functional groups
CN	1	803 cm^{-1}	Breathing mode of s-triazine ring
	2	1230 cm^{-1}	Stretching vibration of C-N-C
	3	1393 & 1538 cm^{-1}	Stretching vibration modes of melem-derived repeating units
	4	1626 cm^{-1}	Deformation mode of NH_2
KPD-CN-7.5	1	803 cm^{-1}	Breathing mode of s-triazine ring
	2	847 & 984 cm^{-1}	P-relevant peak of phosphate
	3	1230 cm^{-1}	Stretching mode of C-N-C
	4	903 & 1146 cm^{-1}	P-O-C stretching
	5	1315 cm^{-1}	Stretching mode of $N-(C)_3$
	6	1404 & 1571 cm^{-1}	Stretching modes of melem-derived repeating units
	7	1628 cm^{-1}	Deformation mode of NH_2
	8	2148 & 2174 cm^{-1}	Cyano group

Table S2. XPS analysis of bare CN and KPD-CN-7.5.[11,16-24]

Sample	Element	No.	Binding energy	Type of bonding
CN	Carbon (C 1s)	C1	284.5eV	C-C; pure graphitic carbon on the amorphous CN matrix or adsorbed hydrocarbon as a contaminant
		C2	285.5eV	R-OH or C-O-C
		C3	286.5eV	C≡N; sp-hybridized carbon
		C4	287.8eV	N-C=N; sp^2-hybridized carbon
		C5	289.2eV	C(O)-O-C or COOH
		C6	293.4eV	N-C-O
	Nitrogen (N 1s)	N1	397.5eV	N-O-C
		N2	398.5eV	C=N-C; sp^2-hybridized nitrogen
		N3	399.8eV	$N-(C)_3$; sp^3-hybridized nitrogen
		N4	401.0eV	C-NHx or C≡N; primary/secondary amine or cyano group
		N5	404.0eV	π-excitations
	Oxygen (O 1s)	O1	531.0eV	Oxygen in carbonyl and carboxylic groups
		O2	532.45eV	-O-; C-OH or N-C-O
		O3	534.4eV	Surface contamination
KPD-CN-7.5	Carbon (C 1s)	C1	284.5eV	C-C; pure graphitic carbon on the amorphous CN matrix or adsorbed hydrocarbon as a contaminant
		C2	288.5eV	R-OH, C-O-C, or C-O-P
		C3	286.5eV	C≡N; sp-hybridized carbon
		C4	288.0eV	N-C=N; sp^2-hybridized carbon
		C5	289.2eV	C(O)-O-C or COOH
		C6	293.4eV	N-C-O
	Potassium (K 2P)	K$2p_{3/2}$	292.6eV	•
		K$2p_{1/2}$	295.4eV	•
	Phosphorus (P 2p)	P *2p*	132.9eV	P-O
	Nitrogen (N 1s)	N1	397.5eV	N-O-C or N-O-P
		N2	398.5eV	C=N-C; sp^2-hybridized nitrogen
		N3	399.8eV	$N-(C)_3$; sp^3-hybridized nitrogen
		N4	401.0eV	C-NHx or C≡N; primary/secondary amine or cyano group
		N5	403.5eV	π-excitations
	Oxygen (O 1s)	O1	531.0eV	Oxygen in carbonyl, carboxylic, or phosphates
		O2	532.45eV	-O-; C-OH, N-C-O, or C-O-P
		O3	534.4eV	Surface contamination

Table S3. XPS elemental composition of bare CN and KPD-CN-x.

	C	N	P	K	O	C/N
	At.%	At.%	At.%	At.%	At.%	
CN	39.16	52.42	0	0	8.42	0.75
KPD-CN-1	39.54	50.09	0.4	1.36	8.62	0.79
KPD-CN-3	38.12	48.61	0.55	2.12	10.61	0.78
KPD-CN-5	36.09	48.04	1.6	2.81	11.46	0.75
KPD-CN-7.5	27.9	42.43	5.69	7.24	16.75	0.66
KPD-CN-10	24.55	43.53	7.21	7.16	17.55	0.56

Table S4. Elemental analysis of bare CN and KPD-CN-x.

	C	N	H	O	C/N
	wt.%	wt.%	wt.%	wt.%	
CN	33.84	62.03	1.32	0.11	0.64
KPD-CN-1	32.45	59.87	0.98	2.26	0.63
KPD-CN-3	27.43	51.46	0.7	4.84	0.62
KPD-CN-5	25	47.74	0.54	6.5	0.61
KPD-CN-7.5	18.85	37.89	0.53	11.65	0.58
KPD-CN-10	19.07	38.59	0.31	10.76	0.58

Table S5. Summary of oxygen-mediated reactions pathways and their standard potentials.[25,26]

No. of eqn.	Reaction pathway	Potential (E^o)
1	$O_2 + H^+ + e^- \rightarrow HO_2$ (acid)	-0.046 V
2	$O_2 + e^- \rightarrow O_2^-$ (alkaline)	-0.33 V
3	$HO_2 + H^+ + e^- \rightarrow H_2O_2$ (acid)	1.44 V
4	$O_2^- + H_2O + e^- \rightarrow HO_2^- + OH^-$ (alkaline)	0.20 V
5	$O_2 + 2H^+ + 2e^- \rightarrow H_2O_2$ (acid)	0.695 V
6	$O_2 + H_2O + 2e^- \rightarrow OH^- + HO_2^-$ (alkaline)	-0.0649 V
7	$O_2 + 4H^+ + 4e^- \rightarrow 2H_2O$ (acid)	1.229 V
8	$O_2 + 2H_2O + 4e^- \rightarrow 4OH^-$ (alkaline)	0.401 V
9	$HO_2 + 3H^+ + 3e^- \rightarrow 2H_2O$ (acid)	1.65 V
10	$O_2^- + 2H_2O + 3e^- \rightarrow 4OH^-$ (alkaline)	0.645 V
11	$H_2O_2 + 2H^+ + 2e^- \rightarrow 2H_2O$ (acid)	1.763 V
12	$HO_2^- + 2e^- + H_2O \rightarrow 3OH^-$ (alkaline)	0.867 V
13	$H_2O_2 + H^+ + e^- \rightarrow OH + H_2O$ (acid)	1.14 V
14	$HO_2^- + H_2O + e^- \rightarrow OH + 2OH^-$ (alkaline)	0.184 V
15	$H_2O + h^+ \rightarrow OH + H^+$ (acid)	2.813 V
16	$OH^- + h^+ \rightarrow OH$ (alkaline)	1.985 V
17	$OH + OH \rightarrow H_2O_2$	-
18	$2H^+ + 2e^- \rightarrow H_2$ (acid)	0.00 V
19	$2H_2O + 2e^- \rightarrow H_2 + 2OH^-$ (alkaline)	0.828 V
20	$CH_3CHO + 2H^+ + 2e^- \rightarrow C_2H_5OH$ (acid)	-0.22 V
21	$2CO_2 + 12H^+ + 12e^- \rightarrow C_2H_5OH + 3H_2O$ (acid)	-0.085 V

Table S6. XPS elemental analysis depending on various chemical reagents employed as precursors.

	C	N	O	P	S	K	Na	Li	Total At.%
	At.%	At.%	At.%	At.%	At.%	At.%	At.%	At.%	
H_3PO_4	38.6	50.2	9.5	1.7	-	-	-	-	100
KH_2PO_4	34.4	47.5	12.1	2.7	-	3.3	-	-	100
K_3PO_4	10.6	33.0	27.8	18.7	-	9.9	-	-	100
H_2SO_4	38.1	53.3	8.6	-	-	-	-	-	100
$KHSO_4$	36.7	50.2	9.4	-	-	3.7	-	-	100
K_2SO_4	34.5	49.6	8.1	-	-	7.8	-	-	100
$(NH_4)H_2PO_4$	37.3	52.2	8.7	1.8	-	-	-	-	100
LiH_2PO_4	37.8	52.1	9.1	1.0	-	-	-	-	100
NaH_2PO_4	34.0	48.8	11.9	2.7	-	-	2.6	-	100
$KHCO_3$	36.0	51.0	8.3	-	-	4.7	-	-	100

References

(1) Fujitsuka, M.; Cho, D. W.; Tojo, S.; Inoue, A.; Shiragami, T.; Yasuda, M.; Majima, T. *J. Phys. Chem. A* **2007**, *111*, 10574-10579.
(2) Bian, Z.; Tachikawa, T.; Zhang, P.; Fujisuka, M.; Majima, T. *J. Am. Chem. Soc.* **2014**, *136*, 458-465.
(3) Gao, H.; Yan, S.; Wang, J.; Huang, Y. A.; Wang, P.; Liad, Z.; Zou, Z. *Phys. Chem. Chem. Phys.* **2013**, *15*, 18077-18084.
(4) Yan, H.; Chen, Y.; Xu, S. *Int. J. Hydrogen Energy* **2012**, *37*, 125-133.
(5) Zhang, J.; Chen, X.; Takanabe, K.; Maeda, K.; Domen, K.; Epping, J. D.; Fu, X.; Antonietti, M.; Wang, X. C. *Angew. Chem.-Int. Edit.* **2010**, *49*, 441-444.
(6) Maeda, K.; Kuriki, R.; Zhang, M.; Wang, X.; Ishitani, O. *J. Mater. Chem. A* **2014**, *2*, 15146-5151.
(7) Kuriki, R.; Sekizawa, K.; Ishitani, O; Maeda, K. *Angew. Chem.-Int. Edit* **2015**, *54*, 2406-2409.
(8) Maeda, K.; Kuriki, R.; Ishitani, O. *Chem. Lett.* **2016**, *45*, 182-184.
(9) Cao, S. W.; Low, J. X.; Yu, J. G.; Jaroniec, M. *Adv. Mater.* **2015**, *27*, 2150-2176.
(10) Khabashesku, V. N.; Zimmerman, J. L.; Margrave, J. L. *Chem. Mater.* **2000**, *12*, 3264-3270.
(11) Liu, J.; Liu, Y.; Liu, N.; Han, Y.; Zhang, X.; Huang, H.; Lifshitz, Y.; Lee, S.-T.; Zhong, J.; Kang, Z. *Science* **2015**, *347*, 970-974.
(12) Miller, F. A.; Wilkins, C. H. *Anal. Chem.* **1952**, *24*, 1253-1294.
(13) Yang, Z. J.; Wang, Z. Q.; Li, J. D.; Chen, J. X. *RSC Adv.* **2012**, *2*, 11432-11437.
(14) Huang, Y.; Wang, Y.; Bi, Y.; Jin, J.; Ehsan, M. F.; Fu, M.; He, T. *RSC Adv.* **2015**, *5*, 33254-33261.
(15) Dong, F.; Wang, Z. Y.; Sun, Y. J.; Ho, W. K.; Zhang, H. D. *J. Colloid Interface Sci.* **2013**, *401*, 70-79.
(16) Vinu, A.; Ariga, K.; Mori, T.; Nakanishi, T.; Hishita, S.; Goberg, D.; Bando, Y. *Adv. Mater.* **2005**, *17*, 1648-1652.
(17) Dong, F.; Sun, Y.; Wu, L.; Fu, M.; Wu, Z. *Catal. Sci. Technol.* **2012**, *2*, 1332-1335.
(18) Martin, D. J.; Qiu, K.; Shevlin, S. A.; Handoko, A. D.; Chen, X.; Guo, Z.; Tang, J. *Angew. Chem.-Int. Edit.* **2014**, *53*, 9240-9245.
(19) Puziy, A. M.; Poddubnaya, O. I.; Socha, R. P.; Gurgul, J.; Wisniewski, M. *Carbon* **2008**, *46*, 2113-2123.
(20) Hu, S.; Li, F.; Fan, Z.; Wang, F.; Zhao, Y.; Lv, Z. *Dalton Trans.* **2015**, *44*, 1084-1092.
(21) Moulder, J. F.; Stickle, W. F.; Sobol, P. E.; Bomben, K. *Handbook of X-ray Photoelectron Spectroscopy*, 2nd ed.; Perkin-Elmer, Physical Electronics Division: Eden Prairie, MN, **1992**.
(22) Gorham, J.; Torres, J.; Wolfe, G.; d'Agostino, A.; Fairbrother, D. H. *J. Phys. Chem. B* **2005**, *109*, 20379-20386.
(23) Zhang, Y. J.; Mori, T.; Ye, J. H.; Antonietti, M. *J. Am. Chem. Soc.* **2010**, *132*, 6294-6295.
(24) Wang, B. B.; Cheng, A. J.; Zhong, X. X.; Wang, Y. Q.; Chen, Y. A.; Ostrikov, K. *J. Appl. Phys.* **2012**, *111*, 044317.
(25) Bard, A. J.; Parsons, R.; Jordan, J. *Standard Potentials in Aqueous Solutions*; IUPAC (Marcel Dekker): New York, 1985.
(26) Danilewicz, J. C. *Am. J. Enol. Vitic.* **2011**, *63*, 1– 10.